Desalination and Water Treatment
www.deswater.com
doi: 10.5004/dwt.2021.27446

232 (2021) 121–128
August

Synthesis and characterization of mesoporous tungsten oxides and application of its photo-catalytic activity on photo-degradation of methyl orange

Seo-Hyun Pak, Chan-gyu Park*

Environmental Technology Division, Korea Testing Laboratory, 87 Digital-ro 26-gil, Guro-gu, Seoul 08389, Korea, Tel. +82-02-860-1105/+82 02-860-1272; Fax: +82-02-860-1689; email: pcg6189@hotmail.com (C.G. Park), Tel. +82-02-860-1139; Fax: +82-02-860-1689; email: seohyunpak@ktl.re.kr (S.-H. Pak)

Received 19 November 2020; Accepted 21 May 2021

ABSTRACT

In this study, mesoporous tungsten oxide was prepared by optimizing the synthesis conditions using P123 as the structure-directing agent, ethanol, and WCl_6. The photo-degradation of methyl orange (MO) was investigated using mesoporous tungsten oxide. The thus-synthesized mesoporous tungsten oxide was characterized by X-ray diffraction (XRD), UV-Vis spectroscopy, nitrogen adsorption-desorption analysis, field emission transmission electron microscope (FE-TEM), Fourier transform infrared spectroscopy and its activity in the photocatalytic degradation of methyl orange was investigated by UV-vis spectroscopy. XRD and FE-TEM analyses confirmed that the synthesized mesoporous tungsten oxide catalysts show homogeneity in mesoporosity, along with higher specific surface area with monoclinic structure. The photo-catalytic efficiency of mesoporous tungsten oxide is controlled by the amount of WCl_6. The results obtained suggest that mesoporous tungsten oxide (W-3) has the highest photo-catalytic performance in the photo-degradation of methyl orange at a shorter time. When the photocatalytic degradation of MO was performed three times, there was no drop in the photocatalytic activity of mesoporous tungsten oxide. As a result, mesoporous tungsten oxide showed that it can be used to decompose organic dye easily, and efficiently and lead to regeneration of the mesoporous tungsten oxide without compromising their performance during reuse test.

Keywords: Mesoporous tungsten oxide; Water treatment; Toxic pollutants; High surface area; Photocatalyst

1. Introduction

Industrial development leads to several environmental problems, and the reduction in environmental pollution is currently a major agenda for international trade. Especially, water pollution is caused by residential waste water, industrial wastewater, etc., causing algal blooms and the death of aquatic organisms [1–3]. A variety of technologies have been suggested to alleviate water pollution and stop the discharge of pollutants; however, water purification is possible only in isolated areas. Physical and chemical treatment technologies such as coagulation, adsorption using activated carbon, membranes and combined coagulation/carbon adsorption system are being established, but the development of pretreatment technologies, such as advanced oxidation process and advanced biological treatment, still require further research for their practical application [4–9].

Water pollution preventive facilities frequently use excess chemical coagulants to meet the strict environmental regulations, causing secondary pollution. Especially, because they have ineffective facilities for the pretreatment of non-biodegradable materials, their treatment efficiencies are low. Moreover, since they frequently run into activated sludge bulking, the biological treatment facilities sometimes fail to operate normally.

* Corresponding author.

Among the various technologies available, photocatalytic technology is considered the most epochal one for removing large quantities of organic pollutants. The most used photocatalysts include TiO_2, Ru^{2+}, ZnO, CdS, SnO_2, and WO_3 [10–13]. There are differences in photoactivity and organic decomposition capacity for each catalyst, currently, TiO_2 is the one used most often. However, if TiO_2 is fastened to a support, the activity and surface area of the catalyst is reduced, it can operate only under UV light, and is easily detachable and deteriorates.

Lately, wide-ranging research is being conducted on oxidized tungsten [14]. Fabrication of photocatalysts with tungsten oxides has been attracting intense interest due to their high chemical stability and narrow band gap energy (2.5–2.8 eV) with proper hole diffusion length [15–16]. However, tungsten oxides as catalysts have shown either a low utilization of solar light, low surface area and faster electron–hole recombination rate [17,18]. Many researchers have extensively studied that mainly structure design with metal doping [19,20], materials compositing and so on. The tungsten oxide nanoparticles with mesoporous structure have high specific surface area and increased photocatalytic activity, so considerable research is ongoing on nanomaterials with porous structure for tungsten oxide.

To prepare mesoporous metal oxides, hard templating and soft templating are normally used. The hard templating method introduces mesoporosity mainly by using Mobil Composition of Matter No. 41 (MCM-41) or Santa Barbara Amorphous type material (SBA-15) as replica. While considerable research has been conducted in this regard, two drawbacks seem to exert strong influence. First, MCM-41 or SBA-15, which is used as replica, has surface area larger than 600; therefore, a mesoporous metal oxide that uses either of them as a replica should have a large surface area, which is not the case in actual studies. According to the reports published by Zamani et al. silica used as a replica has a large surface area of 600–900 $m^2\ g^{-1}$, but the mesoporous metal oxide prepared with it has a surface area of only 40–60 $m^2\ g^{-1}$ [13]. The other drawback of using silica materials is that their removal requires the continuous use of toxic chemicals (e.g., HF), which can hamper mass production [14,21–23]. Therefore, research is ongoing with regard to using poly(ethylene glycol)-block-poly(propylene glycol)-block-poly(ethylene glycol)(pluronic P123) or pluronic F-127 for introducing a structure similar to SBA-15 in metal oxides (MO) [24]. Madhavi et al. [25] reported the structure-directing agent of pluronic-F127 used to introduce a mesoporous structure in NiAl-MO. NiAl-MO with such porous structure showed a specific surface area larger than NiAl-MO prepared in earlier studies and had 4.0 nm cubic pores.

Herein we fabricated tungsten oxide with high surface area and mesoporosity using P123 as the structure-directing agent, ethanol, and tungsten chloride, and tested its catalytic activity and recyclability in the photocatalytic degradation of methyl orange (MO). We observed that the physical properties of mesoporous tungsten oxide were controlled by its synthesis conditions (i.e., solvent, precursor, and P123; in other words, its crystallinity and surface area varied depending on the synthesis conditions, and its responsivity varied accordingly. The synthesized mesoporous tungsten oxide showed excellent photocatalytic activity and reusability for degradation of MO solution.

2. Materials and methods

2.1. Chemicals

P123 (Aldrich®, EO20PO70EO20) was purchased from Sigma-Aldrich. Ethanol and hydrochloric acid was purchased from Samchun Chemical (Korea) and used without purification. Tungsten chloride and methyl orange were purchased from Sigma-Aldrich.

2.2. Syntheses

P123 (Aldrich®, EO20PO70EO20), which was used as a structure-directing agent, was sufficiently melted in ethanol, and was then mixed with a previously prepared mixture of tungsten chloride (WCl_6, Aldrich®) and ethanol. The mixture was stirred at 60°C for 5 min. The composition (weight ratio) of the synthetic solution was tested as shown in Table 1. Then, it was poured into a Petri dish and was treated at 60°C for 24 h. After that the solvent was completely evaporated and obtained powder was calcined up to 350°C using air as a carrier gas (with the temperature rising at 2°C/min) to complete the synthesis of the catalysts.

2.3. Characterization

The crystalline structures of the manufactured catalysts were examined by X-ray diffraction (XRD) analysis (Philips X'pert diffractometer/Cu Kα radiation). UV-vis diffuse reflectance spectroscopy was used to identify the absorbance and intervals among the catalytic strips. The fine structure, shape and size distribution of the catalysts were observed with FE-TEM (JEM-F200 (TFEG) (JEOL Ltd., Japan)). A surface area measurement analyzer (ASAP2000) was used to measure the surface area, pore volume, and distribution of pores of the catalysts. Nitrogen (N_2) full isotherms were measured at 77 K by an ASAP 2020 analyzer (Micromeritics, USA). The surface area of the sample was calculated using the BET (Brunauer–Emmett–Teller) method, and the pore size distribution was determined using the non-local density functional theory method (NLDFT). Tungsten oxide were characterized by attenuated total reflection Fourier transform IR spectroscopy (ATR-FTIR; Nicolet spectrophotometer 5700, Thermo Scientific, MA) with a ZnSe crystal at an incident angle of 45°.

Table 1
Ratio of starting materials

	P123 (g)	Ethanol (mL)	WCl_6 (g)	Temp.(°C)/Time (h)
W-0	0	50	5	60/24
W-1	5		2.5	
W-2			5	
W-3			7.5	

2.4. Photocatalytic activity

To test the photocatalytic activity of the manufactured catalysts, we herein examined the photocatalytic degradation of methyl orange (MO). The initial concentration of the reactants, the added amount of the catalysts, and the amount of the reactant solution were 2 ppm, 0.005 g mL^{-1} and 20 mL, respectively. The reaction setup used included a photo-reactor equipped with 16-W Hg lamp. The reaction setup was made of quartz, and the mixer was installed underneath the reactant device. They were arranged such that a spin bar might be put into the reaction solution during the photocatalytic reaction to prevent sedimentation of the catalyst and to ensure complete mixing. To increase the efficiency of the light source, the reaction setup was wrapped in aluminum foil to keep the light from leaking. Aliquots of the reaction solution was removed at specified intervals of time and was analyzed with a UV-vis spectrophotometer (DR5000, Hach, USA).

3. Results and discussion

3.1. Characterization of mesoporous tungsten oxide as photocatalyst

The process of mesoporous tungsten oxide formation is illustrated in Fig. 1. This involves gradual evaporation of concentrated ethanol from P123, representing a soft template in the solution, forming a homogeneous gel. Slowly evaporating ethanol from a solution containing WO_3, ethanol and P123 promoted the formation of P123-WO_3 linkages, with the mesopores maintained between 7 and 10 nm. These cross-linked P123-WO_3 clusters were also altered during drying.

The XRD spectra of the synthesized mesoporous tungsten, used for identifying its phase structures, are displayed in Fig. 2. The original WO_3 and mesoporous WO_3 samples exhibit the typical monoclinic structure of WO_3 (JCPDS No. 072-1465). The XRD pattern of the original WO_3 and mesoporous WO_3 samples shown in Fig. 2 revealed (0 0 2), (0 2 0), (2 0 0), (1 1 2), (0 2 2), (2 0 2), (0 4 0), (2 4 0) and (2 4 1), which was attributed to the monoclinic phase of WO_3. Those marked with an asterisk are the monoclinic phase of WO_3 in Fig. 2. The crystallinity and crystal structure of the tungsten oxides depend on the calcination temperature, displaying a monoclinic structure below ~350°C, an orthorhombic structure from 350°C to 740°C, and a tetragonal structure above 740°C. Evidently, the W-1, W-2 and W-3 are dominated by the monoclinic structure, with the peaks of the mesoporous WO_3 samples (W-1, W-2 and W-3) being sharper and of higher intensities than those of the W-1.

The FTIR spectra of the WO_x samples prepared with P123 (W-1, W-3) and without P123 (W-0) are shown in Fig. 3. All the samples exhibit strong adsorption between 500 and 1,100 cm^{-1}, characteristic of the stretching modes of W–O bonds in the samples.

In the FTIR spectrum of the mesoporous WO_3 sample (W-3), the peak at 807 cm^{-1} is characteristic of the W–O stretching mode, whereas those at 632 and 578 cm^{-1} are attributed to the O–W–O stretching vibration in WO_3 and stretching vibration of W–O–W in an edge-sharing structure of W_3O_{13}. This peak diminishes progressively, while the main absorption peak at 632 cm^{-1} splits into two peaks at 632 and 578 cm^{-1}, reflective of the WO_3 framework.

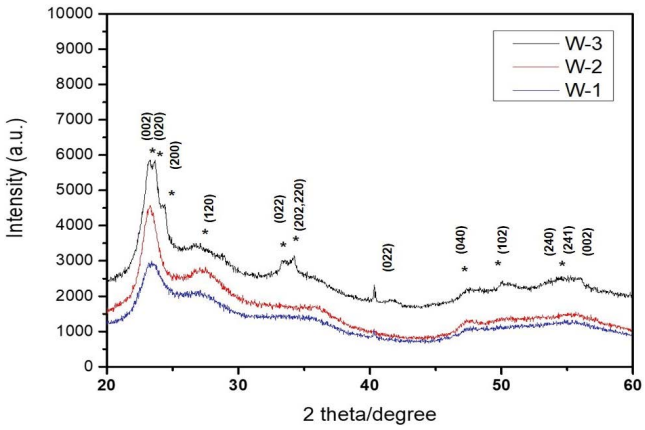

Fig. 2. X-ray diffraction patterns of samples synthesized: W-1, W-2 and W-3.

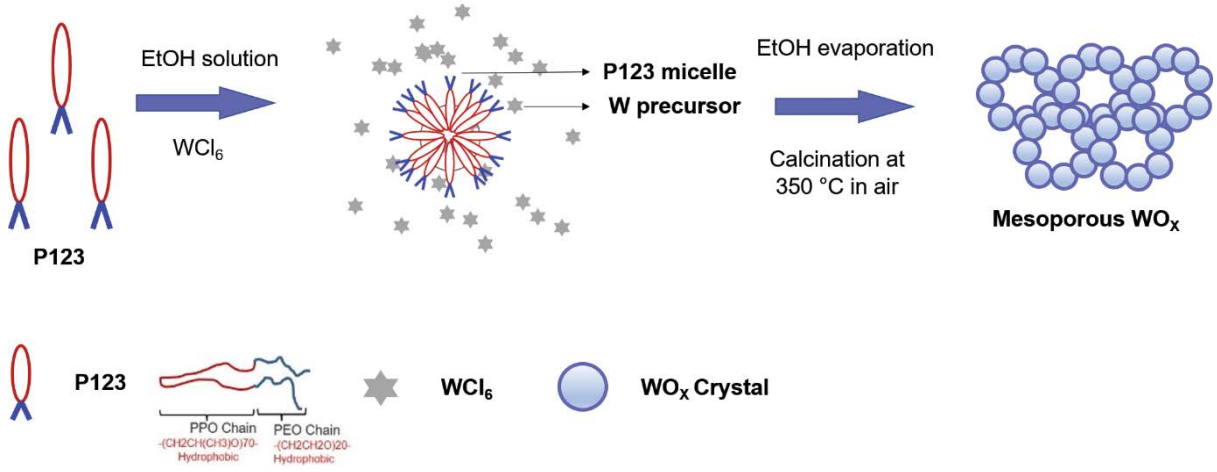

Fig. 1. Scheme of the formation of mesoporous WO_3.

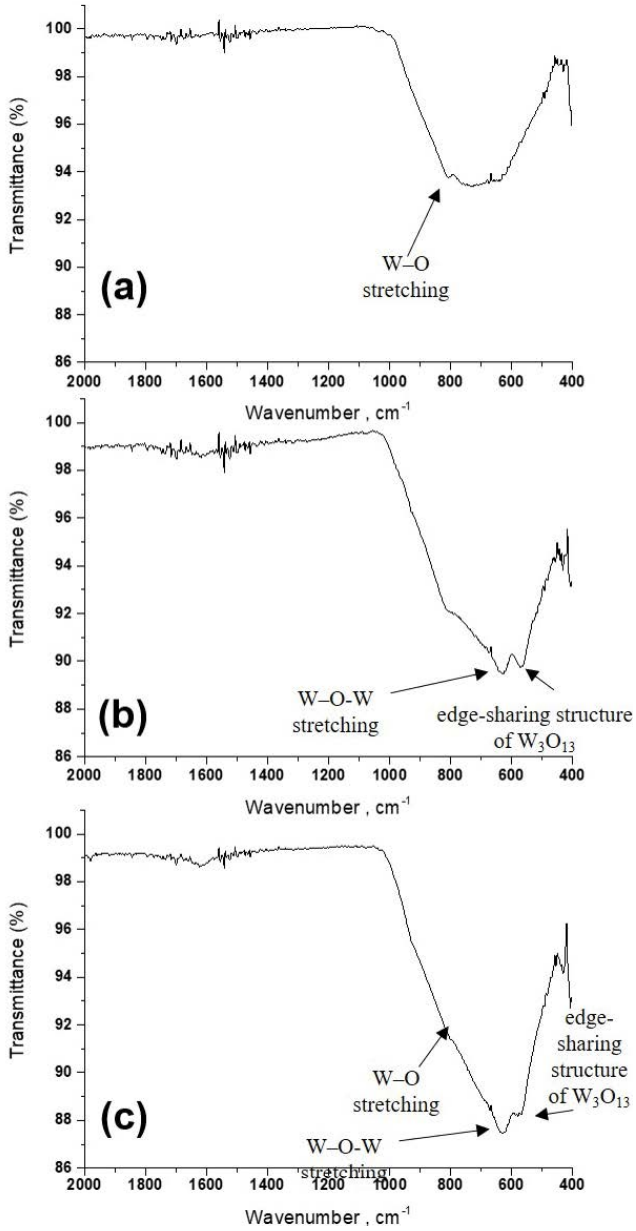

Fig. 3. Fourier transform infrared spectra of samples synthesized: (a) W-0, (b) W-1 and (c) W-3.

In addition, the transmission electron microscope (TEM) images of W-3 (Fig. 4) confirm the WO_3 forms characterized by the monoclinic structure with lattice distances consistent with the (010) plane. In fact, the mesopore lattice spacing of 0.38 nm in the sample corresponds to the spacing of the (010) plane of the monoclinic structure. The TEM analysis also reveals a single-crystal $WO_{2.72}$ structure for the W–C, with growth along the (010) direction.

Further, the UV-Vis absorption spectra of the mesoporous tungsten oxide (W-3) display absorbance starting at ~470 nm, as depicted in Fig. 5. According to the Tauc plot (Fig. 5b), the mesoporous tungsten oxide (W-3) is characterized by a band gap of ~2.40 eV. This value is consistent with the reported range (2.4–2.6 eV) for WO_X nanostructures of different crystal sizes and morphologies [26,27].

The specific surface area of a material is the principal feature controlling its photocatalytic activity. The nitrogen isotherms for the samples represent the type IV isotherm with an H_2 hysteresis loop, further confirming the mesoporosity of the materials (Fig. 6). The BET surface areas of the mesoporous WO_x with different P123 contents and tungsten sources are presented in Table 2. Clearly, the surface area increases with increasing tungsten chloride used in the preparation of the mesoporous samples, with W-3 yielding a value of 228 $m^2 g^{-1}$. This value surpasses that for tungsten oxide from other studies. Calculation of the DFT pore size distribution from the isotherm in Fig. 6b shows two peaks centered at around 7 and 9 nm, while the total pore volume is 0.36 $cm^3 g^{-1}$. For the mesoporous tungsten oxide with a network established during P123 condensation with WCl_6 in ethanol, the P123-WO_3 is linked by the gradually evaporating ethanol, creating the mesopores, which account for the higher surface area than those of other metal oxides. The calcination rate is also an important factor for maintaining the mesopores of the metal oxide. In fact, calcination of the P123-WO_3 composite can cause the mesopores to collapse, thereby reducing the specific surface area. The calcination to 350°C occurred at 2°C min^{-1}, vital for maintaining the mesopores and producing a high surface area.

3.2. Photocatalytic activities of mesoporous tungsten oxide

The effects of the mesoporous nature and surface area on the absorption spectra of dyes in the present samples were investigated. Mixtures of methyl orange (MO) dye

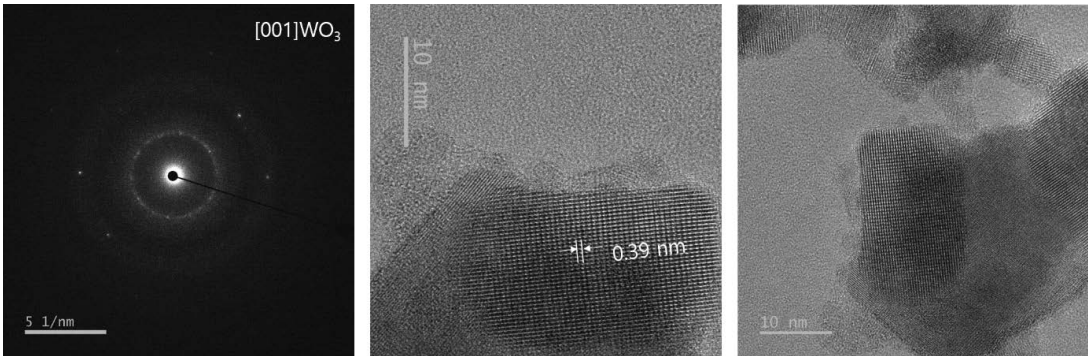

Fig. 4. Transmission electron microscopic images of W-3.

(2 mg L^{-1}) and 80 mg of samples W-0, W-1, W-2, and W-3 were prepared, and the absorption spectra were analyzed at different time intervals. A blank test was conducted under UV irradiation to assess the extent of direct photolysis, with single MO exhibiting negligible photolysis. The UV-Visible spectra of MO reacted with mesoporous tungsten oxide (Fig. 7) shows gradual disappearance of the absorbance peaks of the MO, with complete disappearance after 60 min. The decreased MO absorption band intensities and new peak formation highlight the degradation of the dye in the presence of the mesoporous tungsten oxide catalyst.

The photocatalytic activities of the synthesized W-0, W-1, W-2, and W-3 were then tested by studying MO degradation. The relationship between the presence of mesopores and the degradation efficiency is shown in Fig. 8a). Before turning on the UV source, stirring of the mixture for 20 min after adding the catalyst showed an almost constant concentration. The result for the W-0 sample suggests little change in the MO dye concentration after 60 min irradiation. Conversely, for W-1, W-2, and especially W-3, the MO dye concentration dramatically decreased. Therefore, the photocatalytic activity of the tungsten oxide can be significantly improved by introducing mesopores with a high surface area. As shown in Fig. 8, the degradation efficiency of the tungsten oxide increases as its surface area and mesoporosity increase, varying from 5% to 90% for the MO. The degradation percentage of the MO follows the order W-3 > W-2 > W-1 > W-0. In the case of W-3, the removal rate (%) reached 51% (10 min), 60.5% (20 min), 71.2% (30 min), 90.0% (60 min).

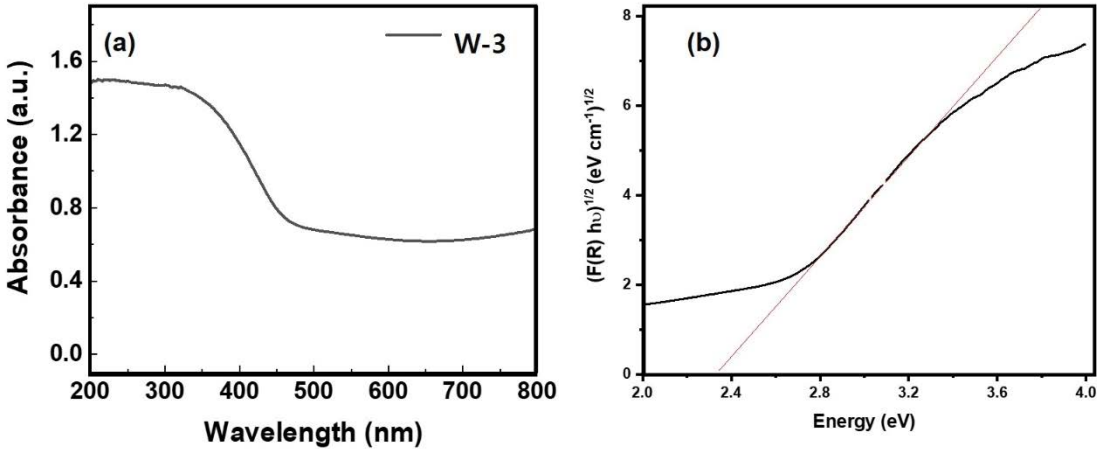

Fig. 5. (a) UV-vis adsorption spectra and (b) Tauc plot of mesoporous tungsten oxide (W-3).

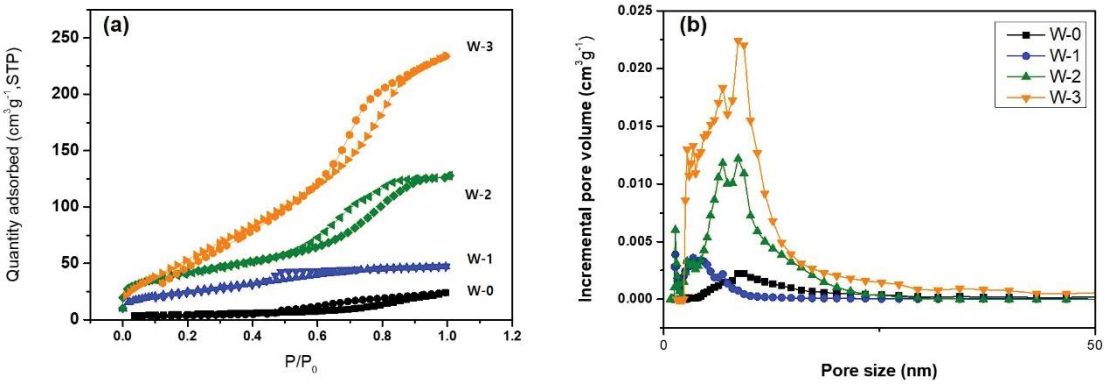

Fig. 6. Nitrogen adsorption/desorption isotherms (a) and DFT pore size distribution of the sample calcined at 350°C (b).

Table 2
Textural properties of the samples prepared with different kind of reaction conditions

	BET surface area	Total pore volume	DFT pore volume (<2 nm)	DFT pore volume (2–300 nm)
W-0	16 $m^2 g^{-1}$	0.030 $cm^3 g^{-1}$	0.001 $cm^3 g^{-1}$	0.029 $cm^3 g^{-1}$
W-1	91 $m^2 g^{-1}$	0.072 $cm^3 g^{-1}$	0.005 $cm^3 g^{-1}$	0.067 $cm^3 g^{-1}$
W-2	147 $m^2 g^{-1}$	0.19 $cm^3 g^{-1}$	0.008 $cm^3 g^{-1}$	0.182 $cm^3 g^{-1}$
W-3	228 $m^2 g^{-1}$	0.36 $cm^3 g^{-1}$	0.02 $cm^3 g^{-1}$	0.345 $cm^3 g^{-1}$

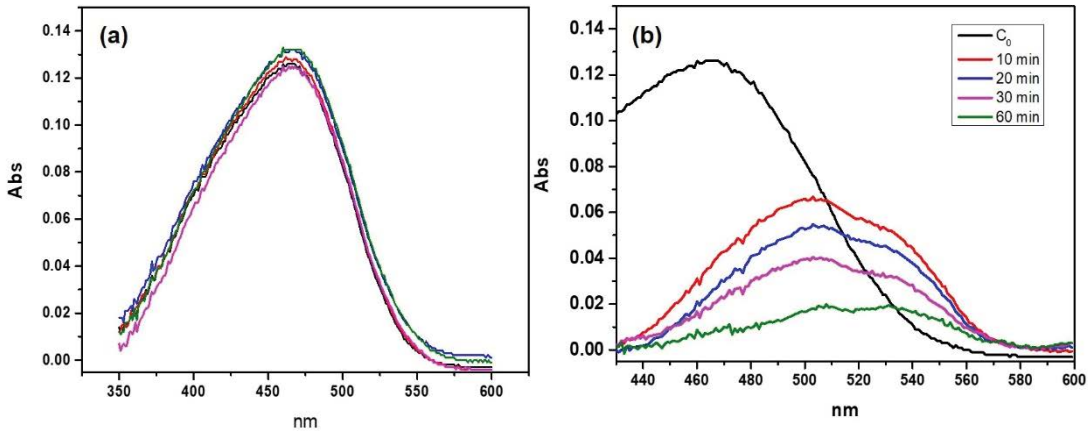

Fig. 7. UV–visible absorbance spectra for the MO solution in the presence of W-0 (a) and W-3 (b) after its exposure to UV light for different times. Experimental conditions: 20.0 mL mixture of MO with 80 mg catalyst.

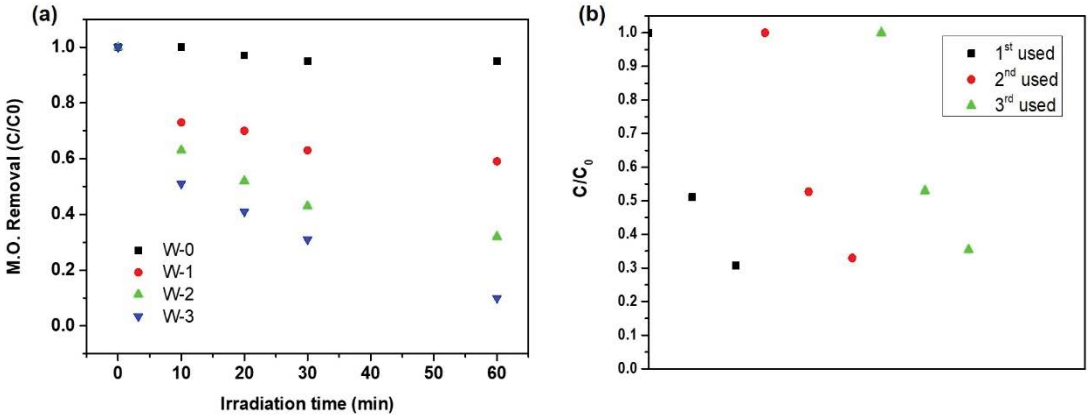

Fig. 8. Photo-degradation efficiency (a) and recycling test (reaction time: 30 min) (b) for MO.

Table 3 shows the comparative removal rate of methyl orange onto catalysts with tungsten oxide. As shown in Table 3, the maximum removal rate of the W-3 is 50 % during 10 min, which is larger than that of most of the reported catalysts.

Based on the above results, it can be explained that high surface area plays important roles for the enhanced photocatalytic activity of W-3. The e^- in the valence band (VB) of tungsten oxide catalysts ware promoted to an empty conduction band (CB). And the electron–hole pairs can move to the W-3 surface and the h^+ reacts with water and hydroxide ions to produce $^{\bullet}OH$ while e^- reacts with oxygen to form hydroxyl radicals. Then, the oxidizing agent, hydroxyl radical, reacts with the MO adsorbed on the W-3 surface.

Recycling tests were conducted over three cycles involving washing of the catalyst three times with deionized water after each run (Fig. 8b). The reuse experiment was allowed to react for only 30 min. This allowed investigation of the photocatalytic activity of the W-3 for MO degradation. The results reveal nearly unchanged catalytic performance, and MO degradation is maintained at around 70% after the three cycles. The slight decreased activity for MO degradation is attributed to intermediates adsorbed on the surface or the collapse of pore channels. In the case of photocatalysts, in addition to efficiency, recyclability and stability are also essential for adsorbent applications. Therefore, W-3, which has the highest photocatalytic activity against MO decomposition, was selected to confirm its recyclability and stability.

4. Conclusions

The purpose of this study was to investigate simple synthesis of mesoporous WO_3 using P123 as a template and evaluate the photocatalytic degradation efficiency of methyl orange through batch tests. The surface area of mesoporous WO_3 is 228 $m^2\ g^{-1}$ and pore size is 7–10 nm, respectively. The photocatalytic activity of mesoporous WO_3 increases from 5% to 90%. The surface area and mesoporosity of the WO_3 as increased, the photocatalytic activity for MO degradation improved. The results explained excellent applicability of as-prepared mesoporous tungsten oxide for the removal of organic dye from water because they could be reused without compromising their performance after repeated degradation process. Also, the present

Table 3
Comparative removal efficiency of organic pollutants onto adsorbents with tungsten oxide

Adsorbent materials	Organic pollutant	Reaction conditions	Removal rate (%)	Ref.
W-3	MO	Catatyst dose: 0.005 g mL^{-1} Reaction time: 10 min Lamp: 16 W Hg lamp	50	Our study
Co_3O_4–$SiPrNH_2$/PW_{12}	MO	Catatyst dose: 0.5 g L^{-1} Reaction time: 10 min Lamp: Not specified	10	[28]
Anodized nanoporous WO_3	MO	Catatyst dose: WO_3 working electrode (3 cm × 4 cm) Reaction time: 20 min Lamp: 500 W xenon lamp	30	[29]
WO_3/Ag_2CrO_4 composites	MO	Catatyst dose: 0.001 g mL^{-1} Reaction time: 40 min Lamp: 300 W Xe-arc lamp	15	[30]
AgBr/WO_3 composite	MO	Catatyst dose: 2 g L^{-1} Reaction time: 20 min Lamp: 500 W Xe lamp	13	[31]

sol-gel method could readily prepare a high surface area of mesoporous tungsten oxide catalysts and they could be separated from the solvent by a simple filtration method.

Acknowledgments

This work is supported by the Korea Agency for Infrastructure Technology Advancement (KAIA) grant funded by the Ministry of Land, Infrastructure and Transport (Grant 20CTAP-C157292-01).

References

[1] A.A. Vaidya, K.V. Datye, Environmental pollution during chemical processing of synthetic fibres, Colourage, 14 (1982) 3–10.
[2] B. Qin, G. Zhu, G. Gao, Y. Zhang, W. Li, H.W. Paerl, W.W. Carmichael, A drinking water crisis in lake Taihu, China: linkage to climatic variability and lake management, Environ. Manage., 45 (2010) 105–112.
[3] S. Vasudevan, M.A. Oturan, Electrochemistry: as cause and cure in water pollution—an overview, Environ. Chem. Lett., 12 (2014) 97–108.
[4] M. Cheng, G. Zeng, D. Huang, C. Lai, Y. Liu, C. Zhang, J. Wan, L. Hu, C. Zhou, W. Xiong, Efficient degradation of sulfamethazine in simulated and real wastewater at slightly basic pH values using Co-SAM-SCS/H_2O_2 Fenton-like system, Water Res., 138 (2018) 7–18.
[5] T. Robinson, G. McMullan, R. Marchant, P. Nigam, Remediation of dyes in textile effluent: a critical review on current treatment technologies with a proposed alternative, Bioresour. Technol., 77 (2001) 247–255.
[6] S. Papić, N. Koprivanac, A. Lončarić Božić, Removal of reactive dyes from wastewater using Fe(III) coagulant, Color. Technol., 116 (2000) 352–358.
[7] S.H. Lin, C.C. Lo, Treatment of textile wastewater by foam flotation, Environ. Technol., 17 (1996) 841–849.
[8] A. Bousher, X. Shen, R.G.J. Edyvean, Removal of coloured organic matter by adsorption onto low-cost waste materials, Water Res., 31 (1997) 2084–2092.
[9] M. Arami, N.Y. Limaee, N.M. Mahmoodi, Investigation on the adsorption capability of egg shell membrane towards model textile dyes, Chemosphere, 65 (2006) 1999–2008.
[10] Z. Huang, Q. Sun, K. Lv, Z. Zhang, M. Li, B. Li, Effect of contact interface between TiO_2 and g-C_3N_4 on the photoreactivity of g-C_3N_4/TiO_2 photocatalyst: (001) vs (101) facets of TiO_2, Appl. Catal., B, 164 (2015) 420–427.
[11] K. Drew, G. Girishkumar, K. Vinodgopal, P.V. Kamat, Boosting fuel cell performance with a semiconductor photocatalyst: TiO_2/Pt-Ru hybrid catalyst for methanol oxidation, J. Phys. Chem. B, 109 (2005) 11851–11857.
[12] M.A. Behnajady, N. Modirshahla, R. Hamzavi, Kinetic study on photocatalytic degradation of C.I. Acid Yellow 23 by ZnO photocatalyst, J. Hazard. Mater., 133 (2006) 226–232.
[13] A.K.L. Sajjad, S. Shamaila, B. Tian, F. Chen, J. Zhang, Comparative studies of operational parameters of degradation of azo dyes in visible light by highly efficient WO_x/TiO_2 photocatalyst, J. Hazard. Mater., 177 (2010) 781–791.
[14] Y. Usami, T. Hongo, A. Yamazaki, Phosphate constituent effects on the structure and photocatalytic properties of mesoporous tungsten oxides, Microporous Mesoporous Mater., 158 (2012) 13–18.
[15] R.U. Meckenstock, M. Elsner, C. Griebler, T. Lueders, C. Stumpp, J. Aamand, S.N. Agathos, H.J. Albrechtsen, Biodegradation: updating the concepts of control for microbial cleanup in contaminated aquifers, Environ. Sci. Technol., 49 (2015) 7073–7081.
[16] Y. Liu, F. Luo, S. Liu, S. Liu, X. Lai, X. Li, Y. Lu, Y. Li, Aminated graphene oxide impregnated with photocatalytic polyoxometalate for efficient adsorption of dye pollutants and its facile and complete photoregeneration, Small, 13 (2017) 1603174, doi: 10.1002/smll.201603174.
[17] X. An, J.C. Yu, Y. Wang, Y.M. Hu, X.L. Yu, G.J. Zhang, WO_3 nanorods/graphene nanocomposites for high-efficiency visible-light-driven photocatalysis and NO_2 gas sensing, J. Mater. Chem., 22 (2012) 8525–8531.
[18] J. Kaur, K. Anand, K. Anand, R.C. Singh, WO_3 nanolamellae/reduced graphene oxide nanocomposites for highly sensitive and selective acetone sensing, J. Mater. Sci., 53 (2018) 12894–12907.
[19] F.G. Wang, C.D. Valentin, G. Pacchioni, Doping of WO_3 for photocatalytic water splitting: hints from density functional theory, J. Phys. Chem. C, 116 (2012) 8901–8909.
[20] D.M. Kabtamu, J.Y. Chen, Y.C. Chang, C.H. Wang, Electrocatalytic activity of Nb-doped hexagonal WO_3 nanowire-modified graphite felt as a positive electrode for vanadium redox flow batteries, J. Mater. Chem. A, 4 (2016) 11472–11480.

[21] E. Kamali, C. Zamani, E. Marzbanrad, B. Raissi, S. Nazarpour, WO_3-based NO_2 sensors fabricated through low frequency AC electrophoretic deposition, Sens. Actuators, B, 146 (2010) 165–170.
[22] P.N. Bhaumik, A soft templating strategy for the synthesis of mesoporous materials: inorganic, organic-inorganic hybrid and purely organic solids, Adv. Colloid Interface Sci., 189–190 (2013) 21–41.
[23] D. Gu, F. Schüth, Synthesis of non-siliceous mesoporous oxides, Chem. Soc. Rev., 43 (2014) 313–344.
[24] Y. Liu, K. Lan, A.A. Bagabas, P. Zhang, W. Gao, J. Wang, Z. Sun, J. Fan, A.A. Elzatahry, D. Zhao, Ordered acro/mesoporous TiO_2 hollow microspheres with highly crystalline thin shells for high-efficiency photoconversion, Small, 12 (2016) 860–867.
[25] P. Madhavi, P. Lakshitha, C.H. Kuo, S. Dharmarathna, S. Suib, Ordered mesoporous mixed metal oxides: remarkable effect of pore size on catalytic activity, Langmuir, 30 (2014) 8228–8237.
[26] F.P. Koffyberg, K. Dwight, A. Wold, Interband transitions of semiconducting oxides determined from photoelectrolysis spectra, Solid State Commun., 30 (1979) 433–437.
[27] G.R. Bamwenda, H. Arakawa, The visible light induced photocatalytic activity of tungsten trioxide powders, Appl. Catal. A, 210 (2001) 181–191.
[28] K. Pourzare, S. Farhadi, Y. Mansourpanah, Anchoring $H_3PW_{12}O_{40}$ on aminopropylsilanized spinel-type cobalt oxide (Co_3O_4-$SiPrNH_2$/$H_3PW_{12}O_{40}$): a novel nanohybrid adsorbent for removing cationic organic dye pollutants from aqueous solutions, Appl. Organomet. Chem., 32 (2017) e4341, doi: 10.1002/aoc.4341.
[29] Q. Zheng, C. Lee, Visible light photoelectrocatalytic degradation of methyl orange using anodized nanoporous WO_3, Electrochim. Acta, 115 (2014) 140–145.
[30] J. Luo, X. Zhou, L. Ma, X. Ning, L. Zhan, X. Xu, L. Xu, L. Zhang, H. Ruan, Z. Zhang, Fabrication of WO_3/Ag_2CrO_4 composites with enhanced visible-light photodegradation towards methyl orange, Adv. Powder Technol., 28 (2017) 1018–1027.
[31] J. Cao, B. Luo, H. Lin, S. Chen, Photocatalytic activity of novel AgBr/WO_3 composite photocatalyst under visible light irradiation for methyl orange degradation, J. Hazard. Mater., 190 (2011) 700–706.